Benchmark Case Study on Mechanical Resistance of Ablated Lower Head Wall during the IVR-ERVC Strategy

Kukhee Lim [a*], Yongjin Cho [a], Yoonhee Lee [a], Jin-Seong Park [a]
[a] Dep. Of Nuclear safety, Korea Institute of Nuclear Safety, 62 Gwahak-ro, Daejeon, Republic of Korea, 34142
[*]Corresponding author: limkh@kins.re.kr

1. Introduction

The lower head wall near the metallic molten pool can be exposed at very high heat flux under ERVC (external reactor vessel cooling) during severe accidents and this is called 'focusing effect'. The heat flux at the ex-vessel is transferred to the coolant by boiling, and the amount of heat flux is limited by CHF (critical heat flux), which is considered as one of the failure criteria of the IVR (in-vessel retention) strategy. On the other hand, the mechanical resistance of the thin ablated wall near the metallic molten pool regardless of CHF is also considered as a failure criterion. Recently, the IVMR(In-Vessel Melt Retention) project by Horizon 2020, which is the R&D strategy of European Commission, has been launched to investigate the application of IVR for 1000 MWe nuclear reactors [1]. The WP2.4 in the project deals with the mechanical resistance of the ablated wall and its benchmark case has been set considering representative plant conditions under ERVC [2]. In this study, the benchmark case is analyzed and the insights from the analysis are proposed.

2. Methods and Results

2.1 Problem Definition of the Benchmark Case

In the benchmark case, the ablated lower head wall and the other part of reactor vessel of the typical 1000 MWe pressurized water reactor shown in Fig. 1 has been modeled. It is assumed that only the wall near the metallic molten pool is ablated because of high heat flux by focusing effect and the thickness of ablated wall is 1.6 cm. To determine the configuration of the ablated wall, thermal load from debris bed considering both of SBO and LB LOCA scenarios are applied. The downward heat flux near the oxidic molten pool is expressed as a function of inclination angle as shown in Eq. (1).

$$\varphi(y) = 0.3 \times 10^6 \times \frac{\theta(y)}{\theta_{max}} \qquad \text{Eq. (1)}$$

where $\varphi(y)$: downward heat flux (W)
y : height from the bottommost part of the lower head (m)
$\theta(y)$: inclination angle (degree)
θ_{max} : maximum angle of the lower head (90°)

The temperatures of the ablated in-vessel wall and the other ex-vessel wall are set to be 1173 K and 373 K respectively. The deadweight of the reactor vessel and corium weight of 180 t are considered. The reactor internal pressure is selected to be 3, 20, 40 and 50 bar in order to check the effect of mechanical loading. The required duration of the analysis is 14 hours.
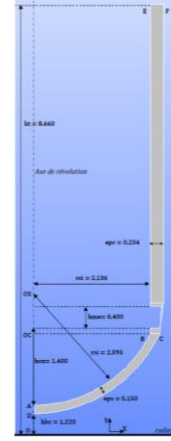
Fig. 1 The geometric configuration of the benchmark case [2]

2.2 Material Properties

The material of the vessel is 16MND5, which is used in French nuclear reactors. The theomophysical properties and tensile properties according to the temperature range from 273 K to 1600 K for the steel material are applied [3]. The creep curves [3] are fitted using the Norton-Bailey model [4] as shown in Eq. (2). The creep coefficient A_T in Eq. (2) is fitted by using the curve fitting tool of ANSYS mechanical APDL for various ranges of temperature and stress and it is compared to SA533B1 steel which is used in the previous studies [5, 6]. The newly fitted A_T is similar to the previously fitted data of SA533B1 steel. And the predetermined values of creep coefficient m in Eq. (2) by the LHF tests [5] as shown in Table. I are used.

$$\dot{\varepsilon}_{cr} = A_T \sigma^m \qquad \text{Eq. (2)}$$

where $\dot{\varepsilon}_{cr}$: creep strain rate (m/m·s)
A_T and m : creep coefficients
σ : stress (Pa)
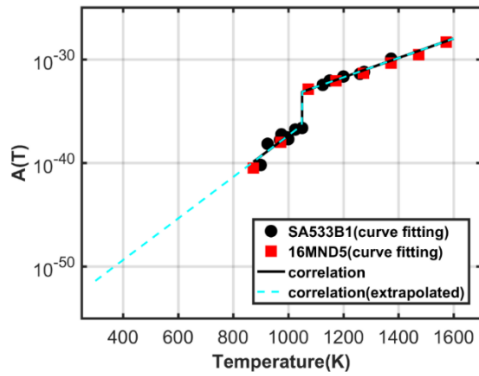
Fig. 2 A_T in Eq. (2) for the lower head steel

Table I: m in Eq. (2) for 16MND5

	T≤1050 K	T>1050 K
m	4.2152	3.6675

Because creep deformation is dominant at temperatures higher than 0.5 T_m [7], where T_m is the melting temperature, the creep curves under 873 K of 16MND5 are not available. However, the temperature of the lower head under ERVC covers low level near the boiling temperature of the ex-vessel coolant, the creep properties at low temperature are also required. In this analysis, A_T under 873 K is linearly extrapolated in logarithmic scale as shown in Fig. 2 using the correlation of A_T in Eq. (3).

$$A_T = 10^{0.0094T} - 42.9784 \quad (T \geq 1050\ K)$$
$$= 10^{0.02T} - 57.4004 \quad (T < 1050\ K) \qquad Eq. (3)$$

2.3 Finite Element Modeling

The detailed finite element (FE) modeling of the ablated reactor vessel with axisymmetric assumption is shown in Fig. 3. The number of elements at the ablated wall is fixed to be 5 in the benchmark case definition. And the coupled thermal and mechanical behavior is analyzed sequentially by using ANSYS mechanical Ver. 18.0. In order to examine the creep deformation, the transient thermal and structural behaviors are analyzed. The element used in the analysis is plane183 with mid-node and the number of elements and nodes are 1685 and 5704 respectively. For the large strain by creep and plastic deformation, geometrical nonlinearity is considered. And the rate-independent plastic behavior is considered using the multi-linear isotropic hardening model. The rate-dependent creep behavior is modeled using the creep model, as shown in Eq. (2).
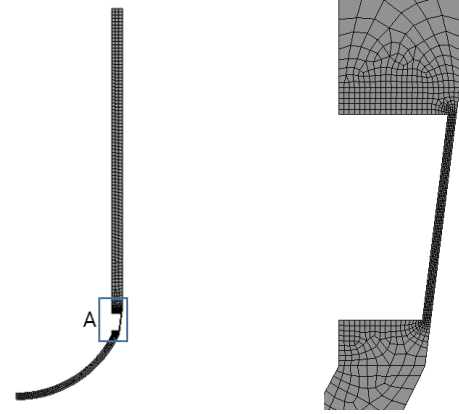
(a) whole geometry   (b) expanded view of part A in (a)
Fig. 3. FE modeling

2.4 Thermal Analysis

The temperature distribution of the reactor vessel at steady state (t = 14 h) according to the thermal boundary conditions is shown in Fig. 4. Based on the temperature distribution at each time step, the mechanical behavior is analyzed.
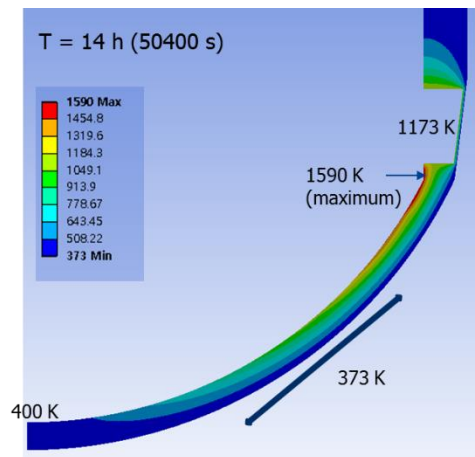
Fig. 4 Temperature distribution (t = 14 h).

2.5 Mechanical analysis

At the internal pressure of 3, 20, 40 and 50 bar, the level of stress and strain are examined at the observation points in Fig. 5. The deformed shape of the thin ablated wall can be characterized by 'ballooning' as shown in Fig. 6.
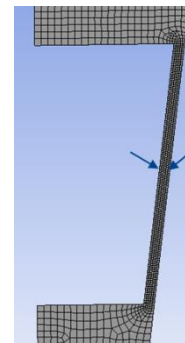
Fig. 5 Observation points for stress and stain
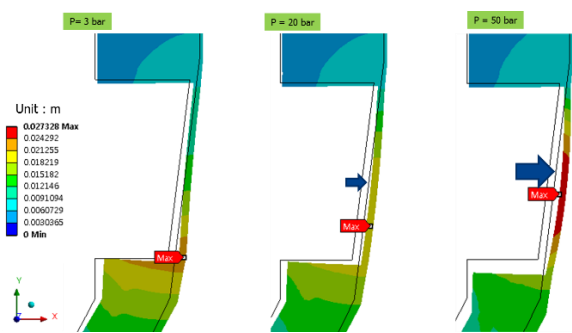
Fig. 6 X-directional displacement by pressure (t = 14 h)

Stress is initially generated by constant deformation from thermal expansion and constant load resulting from internal pressure and strain increases by the stress. Then, stress from constant deformation is relaxed by increase in creep strain at elevated temperature. At P = 20 bar, as shown in Fig. 7, the stress at the in-vessel wall is relaxed to the elastic range. At P = 50 bar, as shown in Fig. 8, stress at the in-vessel wall is also significantly relaxed. However, stress at the ex-vessel wall increases by stress redistribution. This means that creep can also affect the stress at the ex-vessel region. If creep is not considered, the stress at the in-vessel wall approaches to ultimate strength as shown in Fig. 7 and 8 and it may result in failure.

The stress at the in-vessel wall in Fig. 9 is relaxed under the yield strength at the all pressure levels. However, the stress at the ex-vessel wall in Fig. 9 is near the plastic range. The increase in internal pressure generally results in the stress increase even up to the plastic range. And the high stress at the ex-vessel wall comparing to the low stress at the in-vessel wall means that the stiffness of the ablated wall is maintained mainly by the ex-vessel wall region with plastic deformation.

Plastic strain in Fig. 10 is generated when stress is in plastic range. The high plastic strain at the in-vessel wall is mainly generated before stress relaxation at the initial stage. At low pressure (P ≤ 20 bar), the level of plastic strain is similar and is less than 2 %. At high pressure (P ≥ 40 bar), plastic strain is high at the ex-vessel wall. Creep strain in Fig. 11 is high at the in-vessel wall by high temperature. And the increase in stress by pressure in Fig. 9 affect the increase in creep strain. The high creep strain at low pressure is mainly generated before stress relaxation at the initial stage as shown in Fig. 12.

Actually, because stress at the in-vessel wall with low pressure are significantly relaxed, the creep strain rate (slope of creep strain) becomes very low as shown in Fig. 12. However, at high pressure, creep strain increases by time continuously. This may result in very high strain at the long-term behavior which leads to failure.
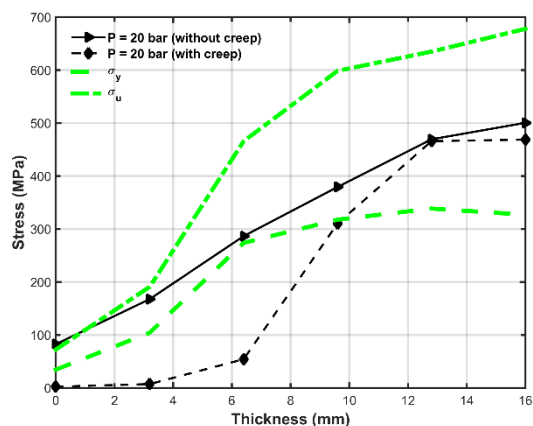
Fig. 7 Equivalent stress by creep consideration (P = 20 bar, t = 14 h)
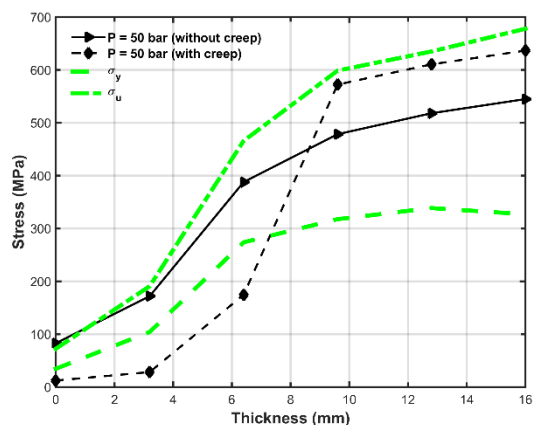
Fig. 8 Equivalent stress by creep consideration (P = 50 bar, t = 14 h)
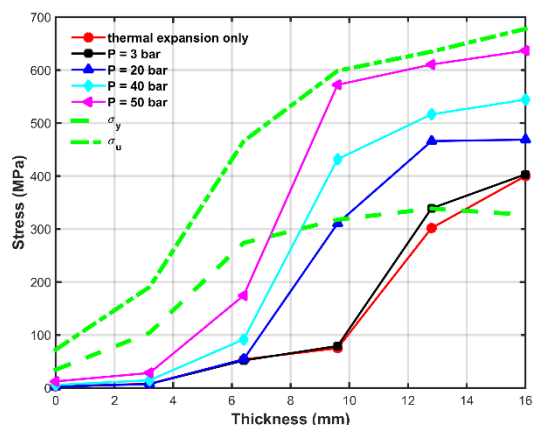
Fig. 9 Equivalent stress by pressure (t = 14 h)
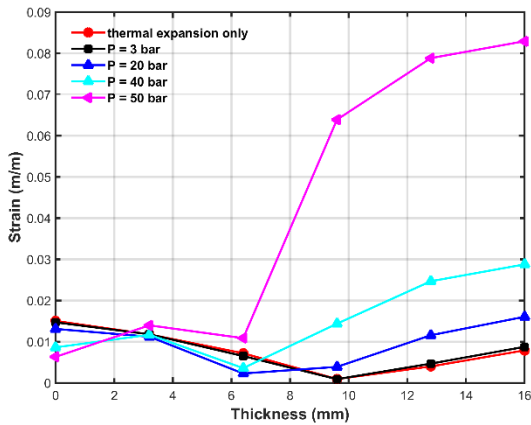
Fig. 10 Equivalent plastic strain by pressure (t = 14 h)
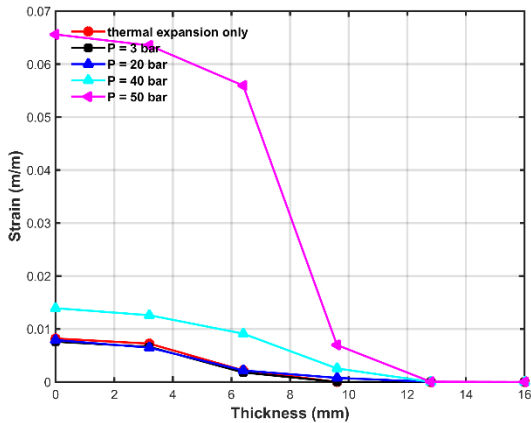
Fig. 11 Equivalent creep strain by pressure (t = 14 h)
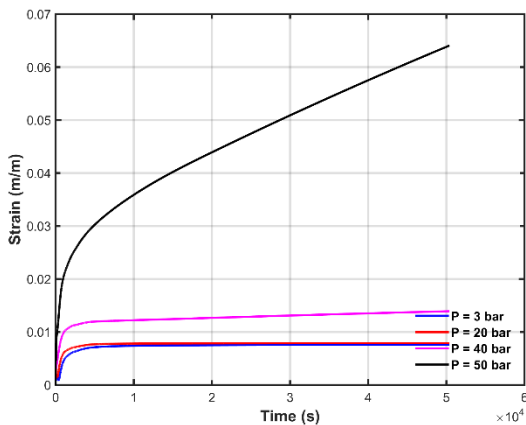
Fig. 12 Equivalent creep strain by pressure (transient, in-vessel wall)

3. Conclusions

The reactor lower head under ERVC ablated by focusing effect experiences stress relaxation or redistribution by creep deformation. That is, the stress level at the in-vessel wall is relaxed from ultimate strength to the elastic range. And because the ex-vessel wall with low temperature has high strength, the stiffness

of the ablated wall is sustained by plastic deformation of the ex-vessel wall area without experiencing creep deformation. Because the plastic deformation is rate-independent, the low level of strain is maintained at the steady state with zero creep strain rate. This is typical at low internal pressure. However, at high internal pressure, the stress at both of the in- and ex-vessel walls becomes relatively high, which results in high creep strain at the in-vessel wall and high plastic strain at the ex-vessel wall. The constant creep strain at high internal pressure can result in stress distribution, even at the ex-vessel wall.

ACKNOWLEDGEMENTS

REFERENCES

[1] F. Fichot et al., "First periodic activity report", IVMR project internal report, 2016.
[2] S. Jules, L. Flandi and K. Atkhen, Structural assessment of a generic PWR1000 reactor vessel under IVR, IVMR project internal report, 2016.
[3] H.-G. Willschutz and E. Altstadt, "Generation of a High Temperature Material Data Base and its Application to Creep Tests with French or German RPV-steel", FZR-353, 2002.
[4] F. H. Norton, "The creep of steel at high temperature", McGraw-Hill, 1929.
[5] T. Y. Chu, et al., "Lower Head Failure Experiments and Analyses", Sandia National Laboratories, NUREG/CR-5582, 1999.
[6] Kukhee Lim, First result of the benchmark case of mechanical behavior of ablated wall, IVMR 3rd annual meeting, May 28-30, Rez, Czech Rep., 2018.
[7] J. Pellg, "Mechanical properties of materials", Springer Science & Business Media, 2012.